Impact of dynamic subgrid scale modeling in variationalmultiscale large-eddy simulation of bluff-body flows

Carine Moussaed, Stephen Wornom, Maria Vittoria Salvetti, Bruno Koobus, Alain Dervieux

Standard J. 12: 345–678 (2013)
DOI 10.1007/s00815-002-6789-z

GENERIC ARTICLE CATEGORY

Carine Moussaed · Stephen Wornom · Maria-Vittoria Salvetti · Bruno Koobus · Alain Dervieux

Impact of dynamic subgrid scale modeling in variational multiscale large-eddy simulation of bluff-body flows

the date of receipt and acceptance should be inserted later

Abstract The effects of dynamic subgrid scale (SGS) modeling are investigated in variational multiscale (VMS) LES simulations of bluff-body flows. The spatial discretization is based on a mixed finite element/finite volume formulation on unstructured grids. In the VMS approach used in this work, the separation between the largest and the smallest resolved scales is obtained through a variational projection operator and a finite volume cell agglomeration. The dynamic and non-dynamic versions of Smagorinsky and WALE SGS models are used to account for the effects of the unresolved scales. In the VMS approach, these effects are only modeled in the smallest resolved scales. The VMS-LES and classical LES approaches, combined with the considered dynamic and non-dynamic SGS models, are applied to the simulation of the flow around a circular cylinder at Reynolds numbers 3900 and 20000 and to the flow around a square cylinder at Reynolds numbers 22000 and 175000.

Keywords variational multiscale LES · dynamic SGS model · unstructured grids · circular cylinder · square cylinder.

1 Introduction

Nowadays, thanks to the increasing availability of large computational resources, large-eddy simulation (LES) is widely used also for industrial and engineering applications, e.g. for the simulation of turbulent flows characterized by complex realistic geometries and by a dynamics involving a wide range of time and space scales. The basic idea of LES is to directly simulate the turbulence scales larger than a given size, usually related to the grid resolution, while the effects of the neglected smaller scales is provided by a closure model (see e.g. [1] for an introduction). The success of a LES depends on different factors, viz. grid resolution and topology, closure modeling and numerics. For all these aspects, the simulation of complex engineering or industrial flows may lead to different choices compared to those mostly adopted in well assessed LES of academic flows. For instance, complex geometries usually lead to the use of anisotropic and non-homogeneous grids, possibly

C. Moussaed · B. Koobus
I3M, Université Montpellier 2, Place Eugène Bataillon, 34095 Montpellier cedex, France
E-mail: carine.moussaed@univ-montp2.fr, koobus@math.univ-montp2.fr

S. Wornom
LEMMA, 2000 Route des Lucioles, 06902 Sophia-Antipolis, France
E-mail: Stephen.Wornom@inria.fr

M.V. Salvetti
Dipartimento di Ingegneria Civile e Industriale, Università di Pisa, Via G. Caruso 8, 56122 Pisa, Italy
E-mail: mv.salvetti@dia.unipi.it

A. Dervieux
INRIA, 2004 Route des Lucioles, 06902 Sophia-Antipolis, France
E-mail: alain.dervieux@sophia.inria.fr

unstructured. Moreover, due to the flow complexity and to the need of limiting computational costs, low-order robust numerical schemes are often adopted together with *cheap* subgrid scale (SGS) models.

The present work is part of a research activity aimed at developing and validating methodologies for the application of LES to flows of industrial or engineering interest. We adopted an approach based on the following key ingredients: (i) unstructured coarse grids, (ii) a second-order accurate numerical scheme stabilized by an ad-hoc developed numerical viscosity, and (iii) the variational multiscale (VMS) formulation combined with non-dynamic eddy-viscosity SGS models. These choices have been extensively discussed and investigated in our previous publications (see, e.g, [2]-[4]) and the main features are only briefly recalled in the following.

The numerical method is based on a mixed finite-volume/finite-element discretization, applicable to unstructured grids, combined with linearized implicit time advancing. The resulting scheme is second-order accurate in space and time and it is stabilized through a numerical diffusion built with a sixth-order spatial derivative, weighted by the 5th power of local mesh size and by a tunable coefficient [2]. In this way, the impact of this stabilizing term can be reduced as much as possible and it has been a posteriori checked that it does not mask the effect of the SGS model (see e.g. [2–4]). On the other hand, it has also been observed that the numerical viscosity introduced in our formulation is not enough alone to act as a SGS model [3].

Finally, as for the approach to turbulence, we adopted the VMS-LES formulation [5], which is aimed at limiting the effects of the SGS closure model to the smallest resolved scales. The separation between large and small resolved scales was obtained in [5] through Galerkin projection. The VMS idea has some positive implications; in particular, it reduces the excessive dissipation introduced also on the largest resolved scales by non-dynamic eddy-viscosity SGS models, such as, for instance, the Smagorinsky [6] or the Wall-Adapted Local Eddy viscosity (WALE) model [7]. Moreover, it has been observed that the VMS-LES approach also allows the inaccuracies characterizing Smagorinsky-like models near solid walls to be at least partially overcome. But, again, this method has a larger spectrum of potentialities and, since its mechanism concerns a different dimension, it can make a complementary job to a dynamic formulation. The VMS approach is particularly attractive for variational numerical methods and unstructured grids, because it is easily incorporated in such formulations [8] and the additional computational costs with respect to classical LES are very low. We adopted the VMS approach proposed in [8], in which the projection operator in the largest resolved scale space is defined through finite-volume cell agglomeration, and, in our previous studies, we combined it with non-dynamic viscosity models. This kind of models contain a constant, which must be a-priori fixed and which directly controls the amount of introduced SGS dissipation. Therefore, as well known for classical LES, the value of this constant has a remarkable effect on the quality of the results and in most cases it should be space and time dependent. Among the several remedies to this drawback proposed in the literature, the most popular is the dynamic procedure [9], which exploits the information contained in the small resolved scales to compute the SGS model parameter, which is allowed to vary in space and time. This approach is widely used in classical LES and it has been observed in a number of applications that it brings a noticeable improvement in the accuracy of the results compared to non-dynamic SGS modeling. In VMS-LES, the quality of the SGS model is expected to have a more limited impact than for classical LES, as it was indeed found in all our previous studies (e.g. [3,4]). Nonetheless, we also observed that in most cases the introduction of the proper amount of SGS dissipation is a crucial issue also within the VMS-LES approach [3].

Based on the previous observations, the combination of the dynamic procedure, which provides a tuning of the SGS dissipation in space and time, and of the VMS approach, which limits its effects to the smallest resolved scales, appears worth of being investigated. The specific aim of the present work is indeed to investigate the effects of the use of dynamic SGS models within the VMS-LES approach, in combination with the previously outlined numerical ingredients.

Very few dynamic VMS-LES simulations have been performed in the past. A dynamic VMS-LES method was introduced in [10]. A coarse mesh made of macro-cells, defined by an agglomeration process, was used in the variational form brought by the VMS method in order to determine the dynamic SGS model coefficient varying in space and time. This approach is different from the present one, in which the Germano algebraic identity is used independently of the variational formulation. In [10], the test cases of a prolate spheroid and of a forward swept wing were considered. The authors concluded that the proposed dynamic VMS-LES procedure captures small turbulence structures that are not resolved by its static counterpart, but this does not improve significantly integral quantities such as lift and drag predicted by the static VMS-LES method. In the more recent work of Gravemeier [12] a VMS-LES approach is combined with a dynamic Smagorinsky model and with a finite-volume solver in slightly different formulations for the simulation of a turbulent flow in a diffuser. According to this latter work, passing from VMS to dynamic-VMS does not bring a significant improvement. Holmes et al. [11] combined a spectral VMS approach with classical and dynamic versions

of the Smagorinsky model in the simulation of turbulent channel flow. In particular, the sensitivity to the partition between large and small resolved scales was investigated and it was found that the VMS approach in combination with the dynamic Smagorinsky model was significantly less sensitive than in combination with the classical Smagorinsky model.

VMS-LES simulations of bluff-body flows carried out with the Smagorinsky and WALE SGS models as well as with their dynamic counterpart are presented and analyzed herein, in order to appraise the impact of the dynamic procedure on the results. More specifically, we consider the flow around a circular cylinder at Reynolds numbers 3900 and 20000, and the flow around a square cylinder at Reynolds numbers 22000 and 175000. These benchmark flows are well documented in the literature and contain most of the difficulties also encountered in more complex flow configurations of engineering interest.

2 Variational Multiscale LES approach

The VMS formulation consists in splitting between the large resolved scales (LRS) i.e. those resolved on a virtual coarser grid, and the small resolved ones (SRS) which correspond to the finest level of discretization. The VMS-LES method does not compute the SGS component of the solution, but it models its dissipative effects on the SRS, and it preserves the Navier-Stokes model for the large resolved scales.

2.1 VMS formulation

In the present work, we adopt the VMS approach proposed in [8] for the simulation of compressible turbulent flows through a finite volume/finite element discretization on unstructured tetrahedral grids. Let V_{FV} be the space spanned by ψ_k, the finite volume basis function, and V_{FE} the one spanned by ϕ_k, the finite element basis function. In order to separate large and small scales, these spaces are decomposed as: $\psi_k =< \psi_k > +\psi'_k$ and $\phi_k =< \phi_k > +\phi'_k$ where the *brackets* denote a coarse scale and the *prime* a fine scale. Consequently to this decomposition, the flow variables are decomposed as follows:

$$W =< W > +W' + W^{SGS} \tag{1}$$

where $< W >$ are the LRS, W' the SRS and W^{SGS} the unresolved scales. The projection operator based on spatial average on macro-cells defined in [8] is used to compute the basis functions of the LRS space. This, for finite elements, leads to:

$$< \phi_k >= \frac{Vol(C_k)}{\sum_{j\epsilon I_k} Vol(C_j)} \sum_{j\epsilon I_k} \phi_j \tag{2}$$

where $Vol(C_j)$ denotes the volume of C_j, the cell around the vertex j, and $I_k = \{ j/C_j \in C_{m(k)} \}$ where $C_{m(k)}$ is the macro-cell containing the cell C_k. The macro-cells are obtained by a process known as agglomeration [13]. An analogous definition holds for finite-volume basis functions. The SGS model which introduces the dissipative effect of the unresolved scales on the resolved scales is only added to the SRS and it is computed only as a function of the SRS. Therefore, the term below is added to the momentum equations

$$\int_\Omega \tau' \cdot \nabla \Phi' \, d\Omega \tag{3}$$

The SGS stress tensor is expressed herein by means of an eddy-viscosity model and, as previously stated, it is computed as a function of the small resolved scales:

$$\tau'_{ij} = -\mu'_{sgs}(2S'_{ij} - \frac{2}{3}S'_{kk}\delta_{ij}) \; ; \quad S'_{ij} = \frac{1}{2}(\frac{\partial u'_i}{\partial x_j} + \frac{\partial u'_j}{\partial x_i}) \tag{4}$$

where μ'_{sgs} denotes the viscosity of the SGS model used to close the problem, computed as a function of the smallest resolved scales, and u'_i is the i-th component of the SRS velocity. Likewise, the term

$$\int_\Omega \frac{C_p \mu'_{sgs}}{Pr_{sgs}} \nabla T' \cdot \nabla \Phi'_5 \, d\Omega \tag{5}$$

is added to the energy equation. C_p is the specific heat at constant pressure, Pr_{sgs} is the subgrid-scale Prandtl number which is assumed to be constant and T' the SRS temperature.

2.2 SGS viscosities

To obtain the SGS viscosity needed to close the problem, the widely used Smagorinsky model [6] is first considered. In the adopted VMS formulation this writes:

$$\mu'_{\text{sgs}} = < \rho > (C_{\text{S}}\Delta)^2 \, |S'| \quad , \tag{6}$$

where Δ is the filter width, C_{S} is the Smagorinsky coefficient and $|S'| = \sqrt{2S'_{ij}}$. The filter width is defined as the third root of the grid element volume. A typical value for the Smagorinsky coefficient for shear flows is $C_{\text{S}} = 0.1$, which is used herein.

The second SGS model we considered is the Wall-Adapting Local Eddy -Viscosity (WALE) SGS model proposed by Nicoud and Ducros [7]. The eddy-viscosity term in the VMS formulation is defined as follows:

$$\mu'_{\text{sgs}} = < \rho > (C_W\Delta)^2 \frac{((S^d_{ij})'(S^d_{ij})')^{\frac{3}{2}}}{(S'_{ij}S'_{ij})^{\frac{5}{2}} + ((S^d_{ij})'(S^d_{ij})')^{\frac{5}{4}}} \tag{7}$$

with $(S^d_{ij})' = \frac{1}{2}({g'_{ij}}^2 + {g'_{ji}}^2) - \frac{1}{3}\delta_{ij}{g'_{kk}}^2$ being the symmetric part of the tensor ${g'_{ij}}^2 = g'_{ik}g'_{kj}$, where $g'_{ij} = \partial u'_i/\partial x_j$. As indicated in [7], the constant C_W is set to 0.5.

2.3 Dynamic model

In their original formulations, C_{S} and C_W appearing in the expression of the viscosity of the Smagorinsky and WALE SGS model (Eqs. (6) and (7) respectively) are set to a constant over the entire flow field and in time. In the dynamic model [9], this constant is replaced by a dimensionless parameter $C(x,t)$ that is allowed to be a function of space and time. The dynamic approach also provides a systematic way for adjusting this parameter in space and time by using information from the resolved scales. After the introduction of the grid filter, denoted by *overline* and *tilde*, *tilde* being Favre averaging, $\tilde{f} = \overline{\rho f}/\overline{\rho}$, a second filter is considered, having a larger width than the grid one, which is called the test-filter and denoted by a *hat*. The test-filter is applied to the grid-filtered Navier-Stokes equations, and then, the subtest-scale stress is defined as follows:

$$M^{test}_{ij} = \widehat{\overline{\rho\mathbf{u}_i}\overline{\mathbf{u}_j}} - \left(\hat{\bar{\rho}}\right)^{-1}\left(\widehat{\overline{\rho\mathbf{u}_i}}\,\widehat{\overline{\rho\mathbf{u}_i}}\right) \tag{8}$$

The deviatoric part of M^{test}_{ij} can be written using a Smagorinsky or WALE model, as

$$M^{test}_{ij} - \frac{1}{3}M^{test}_{kk}\delta_{ij} \;=\; -C\hat{\Delta}^2\hat{\bar{\rho}}g(\hat{\tilde{\mathbf{u}}})\hat{\tilde{P}}_{ij} \quad (C \;=\; {C_W}^2 \text{ or } {C_{\text{S}}}^2) \tag{9}$$

with $\hat{\tilde{P}}_{ij} = -\frac{2}{3}\hat{\tilde{S}}_{kk}\delta_{ij} + 2\hat{\tilde{S}}_{ij}$ and where $g(\hat{\tilde{\mathbf{u}}})$ denotes the contribution to the SGS viscosity depending on the gradient velocity that appears in (6) for the Smagorinsky model, and in (7) for the WALE model. The constant C, as originally proposed in [9], is assumed to be constant at the subgrid and subtest levels.

By using the Germano identity [9] and a least-square approach [14] to contract the resulting tensorial equation, we obtain:

$$(C\Delta^2) = \frac{L_{ij}B_{ij}}{B_{pq}B_{pq}} \tag{10}$$

where:

$$L_{ij} = \mathcal{L}_{ij} - \frac{1}{3}\mathcal{L}_{kk}\delta_{ij}\;; \quad \mathcal{L}_{ij} = \widehat{\bar{\rho}\tilde{\mathbf{u}}_i\tilde{\mathbf{u}}_j} - \left(\hat{\bar{\rho}}\right)^{-1}\left(\widehat{\bar{\rho}\tilde{\mathbf{u}}_i}\widehat{\bar{\rho}\tilde{\mathbf{u}}_i}\right) \tag{11}$$

and

$$B_{ij} \;=\; \widehat{\bar{\rho}g(\tilde{\mathbf{u}})\tilde{P}_{ij}} - \left(\frac{\hat{\Delta}}{\Delta}\right)^2 \hat{\bar{\rho}}g(\hat{\tilde{\mathbf{u}}})\hat{\tilde{P}}_{ij}. \tag{12}$$

Note that all quantities in the right-hand side of Eq. (10) are known from the LES computation. Note also that we preferred to dynamically compute $(C\Delta^2)$, instead of C as done in the original dynamic procedure, in order to partially overcome difficulties in the definition of the filter width for inhomogeneous and unstructured grids.

Finally, as done also in [11], the classical dynamic procedure previously briefly outlined, which involves all the resolved scales, is used herein. Once $(C\Delta^2)$ is dynamically computed, it is injected in Eq. (6) or (7) to obtain the SGS viscosity used in the VMS approach.

A possible drawback of the dynamic procedure based on the Germano-identity [9] when applied to a SGS model already having a correct near-wall behavior, as the WALE one, is the introduction of a sensitivity to the additional filtering procedure. A simple way to avoid this inconvenient is to have a sensor able to detect the presence of the wall, without a priori knowledge of the geometry, so that the dynamic SGS model adapts to the classical constant of the model, which is equal to 0.5 in the near wall region for the WALE model, and compute the constant dynamically otherwise. We adopt the sensor proposed in [15], having the following expression:

$$SVS = \frac{(\widetilde{S_{ij}}^d \widetilde{S_{ij}}^d)^{\frac{3}{2}}}{(\widetilde{S_{ij}}^d \widetilde{S_{ij}}^d)^{\frac{3}{2}} + (\widetilde{S_{ij}}\widetilde{S_{ij}})^3}. \tag{13}$$

This parameter has the properties to behave like y^{+3} near a solid wall, to be equal to 0 for pure shear flows and to 1 for pure rotating flows.

It should be noticed that the implementation of the dynamic SGS models in our software has been optimized so that the additional cost of the resulting dynamic LES and VMS models, in the case of an implicit time-marching scheme, which is our default option, is less than 1% compared to their non-dynamic counterparts.

3 Numerical discretization

We briefly recall now the main features of the numerical scheme. Further details can be found in [2] and in [16].

The governing equations are discretized in space using a mixed finite volume/finite element method applied to unstructured tetrahedrizations. The adopted scheme is vertex centered, i.e. all degrees of freedom are located at the vertices. P1 Galerkin finite elements are used to discretize the diffusive terms.

A dual finite-volume grid is obtained by building a cell C_i around each vertex i; the finite-volume cells are built by the rule of medians: the boundaries between cells are made of triangular interface facets. Each of these facets has a mid-edge, a facet centroid, and a tetrahedron centroid as vertices. The convective fluxes are discretized on this tessellation by a finite-volume approach, i.e. in terms of the fluxes through the common boundaries between each couple of neighboring cells. The unknowns are discontinuous along the cell boundaries and this allows an approximate Riemann solver to be introduced. The Roe scheme [17] (with low-Mach preconditioning) represents the basic upwind component for the numerical evaluation of the convective fluxes. The MUSCL linear reconstruction method ("Monotone Upwind Schemes for Conservation Laws"), introduced by Van Leer [18], is adapted for increasing the spatial accuracy. The basic idea is to express the Roe flux as a function of reconstructed values of W at the boundary between two neighboring cells. Attention has been dedicated to the dissipative properties of the resulting scheme which is a key point for its successful application to LES simulations.The numerical dissipation in the resulting scheme is made of sixth-order space derivatives by using suited reconstructions [2]. Moreover, a tunable parameter, γ, directly controls the amount of introduced numerical viscosity and this allows to reduce it to the minimal amount needed to stabilize the simulation. Time advancing is carried out through an implicit linearized method, based on a second-order accurate backward difference scheme and on a first-order approximation of the Jacobian matrix [19]. The resulting numerical discretization is second-order accurate both in time and space.

4 Applications

4.1 Circular cylinder flow at Reynolds number 20000

Let us start by presenting the results of the simulations of the flow around a circular cylinder carried out at Reynolds number based on the cylinder diameter, D, and on the freestream velocity, Re, equal to 20000. The computational domain is such that $-10 \leq x/D \leq 25$, $-20 \leq y/D \leq 20$ and $-\pi/2 \leq z/D \leq \pi/2$, where x, y and z denote the streamwise, transverse and spanwise directions respectively, the cylinder axis being located at $x = y = 0$. Periodic boundary conditions are applied in the spanwise direction while no-slip conditions are imposed on the cylinder surface. Characteristic based conditions are used at the inflow and outflow as well as

on the lateral surfaces ($y/D = \pm 20$) [20]. The freestream Mach number is set equal to 0.1 in order to make a sensible comparison with incompressible simulations in the literature. Preconditioning is used to deal with the low Mach number regime. The computational domain is discretized by an unstructured grid consisting of approximately 1.8 million of nodes. The averaged normal distance of the nearest point to the cylinder boundary is 0.001D, 320 nodes are uniformly distributed on the cylinder surface in the azimuthal direction and 100 nodes are present in the spanwise direction near the cylinder, with an approximately uniform distribution. The computational domain, boundary conditions and grid are the same as in [4]. As for the remaining simulation parameters, the coefficient controlling the numerical viscosity is set to 0.3, chosen on the basis of previous sensitivity studies [3]. Finally, the time step, adimensionalized with the freestream velocity and the cylinder diameter, is equal to 2.5×10^{-4}; therefore, a vortex shedding period contains approximately 500 time steps. LES and VMS-LES simulations have been carried with this set up for the WALE and the Smagorinsky SGS models in their original formulation as well as in their dynamic version. The results of a simulation carried without any explicit SGS model are also reported, in order to highlight the effects of the SGS terms compared to those of numerical viscosity.

First of all, the dynamic procedure has a remarkable effect on the amount of introduced SGS viscosity. In all the considered cases, the SGS viscosity produced in the wake by dynamic SGS models is significantly reduced compared to that given by their non-dynamic counterparts. An example is given in Figure 1, showing the instantantaneous iso-contours of μ_{sgs}/μ obtained in the VMS-LES simulations with the non-dynamic and dynamic WALE models respectively.

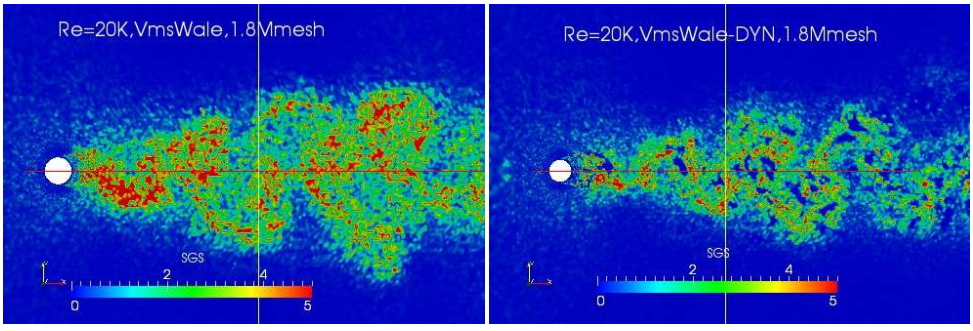

Fig. 1 Flow around a circular cylinder at Reynolds 20000 : viscosity ratio for the VMS-WALE (left) and for dynamic VMS-WALE (right).

The impact of these differences in SGS viscosity is investigated in terms of flow bulk parameters and statistics. For all simulations, statistics are computed by averaging in the spanwise homogeneous direction and in time for 35 vortex shedding cycles. The main bulk coefficients and quantities of interest are summarized in Table 1. They are compared with the experimental results of [23] and [24] and with the data of the review in [25]. As for simulations, we recall the LES results of [22] and of [21]. In [22] an implicit LES simulation, i.e. without any explicit SGS model, was carried out on a grid of 2.3×10^6 cells, while the LES in [21] were carried out for different grid resolutions, the most refined one having about 5×10^5 nodes, and with dynamic Smagorinsky and mixed models. The range of values of the considered quantities obtained in the different simulations in [21] is reported in Table 1.

As a first remark, the Strouhal number, i.e. the vortex-shedding frequency made non dimensional with the cylinder diameter and the freestream velocity, is practically not sensitive to SGS modeling and, in all cases, in good agreement with the experimental data taken from [25]. In general, we observed that this quantity is well predicted in all the considered LES or VMS-LES simulations of the circular cylinder flow (see the results in Sec. 4.2 and in [4] for Re=3900 and Re=10000).

As for the mean drag coefficient, all the numerical predictions are inside the experimental range, except for the ones given by the simulation with no SGS model and the LES one with the Smagorinsky model, characterized by an overestimation of $\overline{C_d}$ of 7.5% and of 5%, compared to upper limit of the experimental range, respectively. These two simulations also give the largest discrepancies from the experimental value of [25] in the prediction of the r.m.s. of the time fluctuations of the lift coefficient, C'_L, with an overestimation of 31% for the simulation with the Smagorinsky model and of 29% for the one with no model. These results first confirm the inadequacy of numerical viscosity in our formulation to replace a phyically based SGS model,

	$\overline{C_d}$	C'_L	l_r/D	$\text{-}\overline{C_{pb}}$	St	L_V/D	$I(\%)$
LES Smagorinsky	**1.29**	**.59**	**.85**	**1.27**	**.19**	**.71**	**34.**
LES dyn. Smagorinsky	**1.21**	**.45**	**.93**	**1.20**	**.19**	**.96**	**34.5**
LES WALE	**1.16**	**.39**	**.97**	**1.15**	**.20**	**.71**	**31.5**
LES dyn. WALE	**1.19**	**.44**	**.92**	**1.16**	**.20**	**.96**	**31.8**
VMS Smagorinsky	**1.18**	**.43**	**.88**	**1.20**	**.20**	**.90**	**32.7**
VMS dyn. Smagorinsky	**1.19**	**.45**	**.95**	**1.19**	**.19**	**1.1**	**36.1**
VMS WALE	**1.17**	**.42**	**.87**	**1.20**	**.20**	**.96**	**33.7**
VMS dyn. WALE	**1.18**	**.43**	**.89**	**1.19**	**.20**	**.96**	**32.8**
no model	**1.26**	**.58**	**.87**	**1.22**	**.20**	**-**	**-**
LES [21] **min.**	**.94**	**.17**	**.55**	**0.83**	–	–	–
max.	**1.28**	**.65**	**1.4**	**1.38**	–	–	–
LES [22]	**1.20**	–	**.99**	**1.25**	–	**.99**	**38.1**
Exp. [23]	**1.16**	–	–	–	–	**1.0**	**37.0**
Exp. [24]	**1.20**	–	–	–	–	–	–
Exp. [25]	–	**.45**	–	**1.19**	**.19**	–	–

Table 1 Main bulk flow parameters and quantities of interest, predicted by dynamic and non-dynamic LES and VMS-LES around a circular cylinder at $Re = 20000$. $\overline{C_d}$ holds for the mean drag coefficient, C'_L for the root mean square of lift time fluctuations, l_r is the recirculation length, $\overline{C_{pb}}$ is the mean pressure coefficient at cylinder basis, St is the Strouhal number, L_V denotes the x-location of the maximum in the turbulent intensity distribution along the wake axis, I holds for the maximum turbulence intensity along the wake axis.

as observed in our previous studies [3,2]. Second, it confirms that the non-dynamic Smagorinsky model in classical LES does not lead to satisfactory predictions also for bulk parameters, while its behavior improves in the VMS-LES approach. The impact of dynamic SGS modeling on the predictions of $\overline{C_d}$ and C'_L is more significant for classical LES than for VMS-LES for both the considered SGS models; in all cases, for these considered parameters, the dynamic SGS models give better or slightly better agreement with the experimental data than their non-dynamic counterparts.

Moving to the analysis of more local quantities, the value of the mean drag is closely related to the mean pressure distribution over the cylinder surface and to the mean base pressure coefficient reported in Table 1. The mean base pressure is defined as the mean pressure at $\theta = 180$, θ being the azimuthal angle, with $\theta = 0$ at the stagnation point. If we consider, for instance, the LES simulation with the Smagorinsky model, it is evident from Table 1 and from Fig. 2(a), showing the distribution of the mean pressure coefficient along the cylinder surface, that the wrong prediction of the mean drag coefficient is due to an underestimation of the mean pressure in the separate wake. It is also evident that the use of the dynamic version improves the agreement between the numerical and experimental values of the mean pressure in the separated wake (see again Fig. 2(a) and Table 1). Conversely, in all the other simulations the effects of the use of the dynamic procedure on the mean pressure distribution are moderate and very small for the VMS-LES ones, as shown for instance in Fig. 2(b) for the WALE model.

Another quantity which is in general rather difficult to be accurately predicted is the length of the mean recirculation bubble, l_r/D; the values obtained in our simulations are reported in Table 1 together with the numerical predictions of [21] and [22]. It appears that the value of l_r/D is quite sensitive to SGS modeling and to the use of the dynamic procedure; our predictions are slightly lower than that of [22] but well inside the range of those of [21], which is, however, quite large. Since we could not find any experimental data for l_r/D at this Reynolds number, no further analysis is carried out here, while the numerical results for l_r/D are discussed more in details in Sec. 4.2 at Re=3900, for which different experimental data are available and this quantity has received large attention in the literature.

Finally, let us focus on the turbulence intensity distribution on the wake centerline. The distributions obtained in LES and VMS-LES simulations with dynamic and non dynamic Smagorinsky model are shown, as an example, in Fig. 3 and compared with the numerical predictions of [22] and with the experimental measurements of [23]. The value and the location of the peak in these distributions, I and L_V/D, are reported in Table 1. The maximum value of the turbulence intensity for all the simulations carried out is underestimated compared to the experimental value. This is however not surprising, since as shown also in Figure 1, the contribution of the SGS model is significant in the very near wake region ($x/D < 2$), and it is not taken into account in the computation of the resolved turbulence intensity. Conversely, the location of the peak, which is related to the length of the vortex formation region [23], should be correctly captured in the simulations. It can

be seen from Table 1 that the use of the dynamic procedure noticeably improves the prediction of L_V/D in all cases, except for the VMS-LES computation with the WALE model, which gives a value in good agreement with the experimental one also for its non-dynamic version.

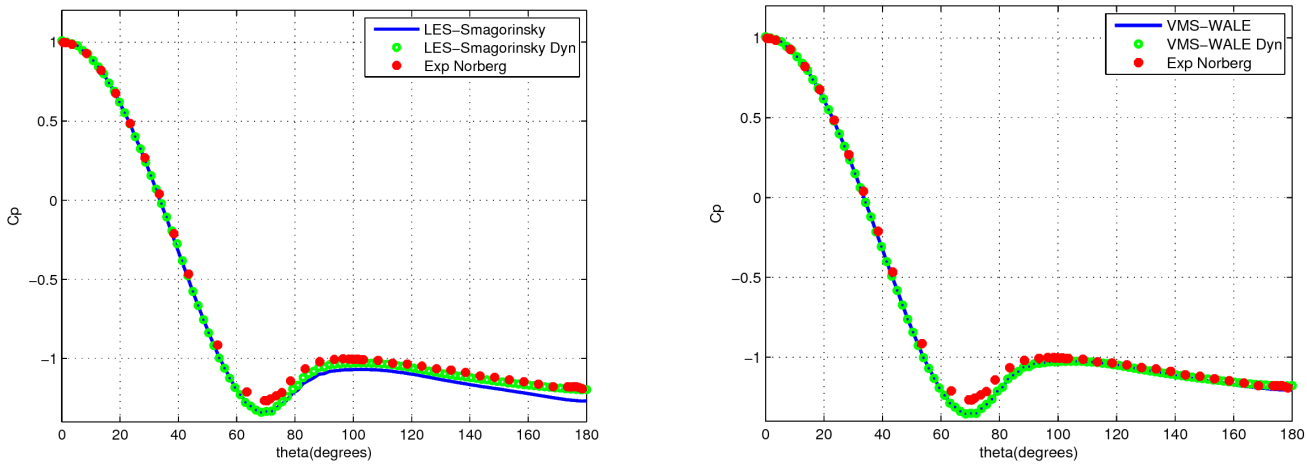

(a) (b)

Fig. 2 Flow around a circular cylinder at Reynolds 20000: mean pressure coefficient distribution at the cylinder from the dynamic and non dynamic LES Smagorinsky (a) and VMS-LES WALE (b) computations.The experimental data are taken from [26].

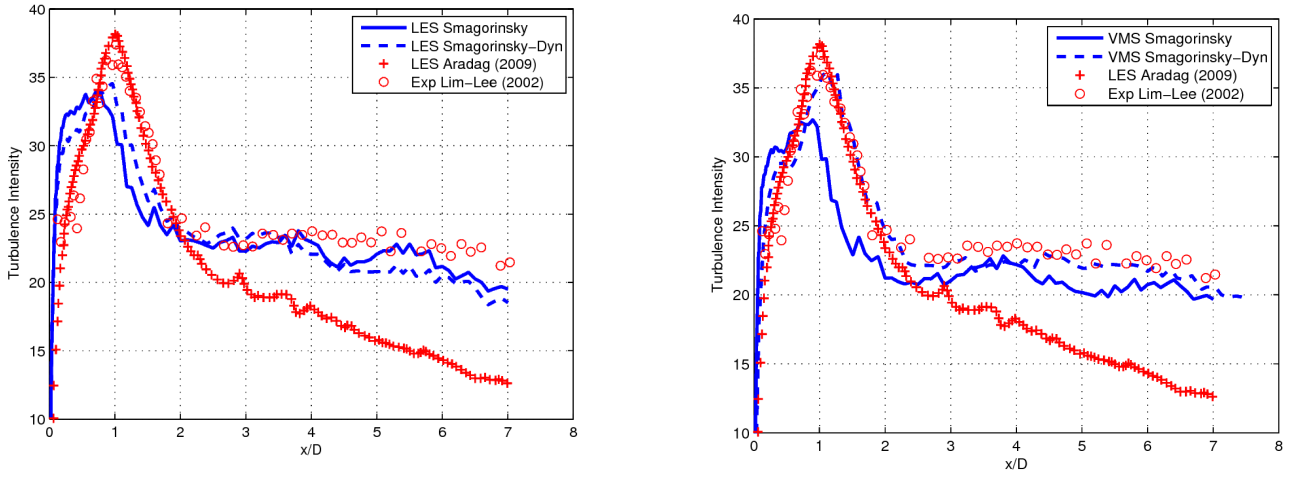

(a) (b)

Fig. 3 Flow around a circular cylinder at Reynolds 20000 : distribution of the turbulence intensity (%) along the wake centerline obtained in LES (a) and VMS-LES (b) simulations with the dynamic and non dynamic Smagorinsky model.The data from [22] and [23] are also reported for comparison.

4.2 Circular cylinder flow at Reynolds number 3900

We consider now flow around a circular cylinder at Re=3900. The computational domain is the same one used for the same flow configuration at Re=20000 in Sec. 4.1. Two different grids are used in this case. The first one (GR1) contains approximately 2.9×10^5 nodes; the averaged distance of the nearest point to the cylinder

boundary is 0.017D, 160 nodes are uniformly distributed on the cylinder surface in the azimuthal direction and 80 nodes are present in the spanwise direction near the cylinder, with an approximately uniform distribution. The second grid (GR2) is obtained from GR1 by refining in a structured way, i.e. by dividing each tetrahedron in 8, resulting in approximately 1.46×10^6 nodes. All the remaining simulation parameters are the same as in Sec. 4.1.

The same averaging procedure as for Reynolds 20000 is used in order to compute the statistics. The main quantities of interest are summarized in Table 2.

	$\overline{C_d}$	l_r/D	$-\overline{Cp_b}$	St
LES Smagorinsky (GR1)	**0.98**	**1.06**	**0.97**	**0.219**
LES dyn. Smagorinsky (GR1)	**0.95**	**1.12**	**0.93**	**0.219**
LES WALE (GR1)	**0.96**	**1.06**	**0.96**	**0.219**
LES dyn. WALE (GR1)	**0.94**	**1.20**	**0.87**	**0.22**
VMS Smagorinsky (GR1)	**0.98**	**1.08**	**0.95**	**0.22**
VMS dyn. Smagorinsky (GR1)	**0.99**	**1.08**	**0.95**	**0.218**
VMS WALE (GR1)	**0.96**	**1.06**	**0.94**	**0.22**
VMS dyn. WALE (GR1)	**0.97**	**1.08**	**0.93**	**0.22**
no model (GR1)	**0.92**	**1.31**	**0.81**	**0.22**
VMS Smagorinsky (GR2)	**0.94**	**1.71**	**0.80**	**0.216**
VMS dyn. Smagorinsky (GR2)	**0.96**	**1.70**	**0.82**	**0.22**
VMS WALE (GR2)	**0.94**	**1.47**	**0.81**	**0.22**
VMS dyn. WALE (GR2)	**0.94**	**1.47**	**0.85**	**0.22**
no model (GR2)	**0.91**	**1.85**	**0.78**	**0.219**
Exp. [27], min.	–	–	–	**0.205**
max.	–	–	–	**0.215**
Exp. [29], min.	–	**1.36**	–	**0.206**
max.	–	**1.66**	–	**0.21**
Exp. Norberg (from [28]), min.	**0.94**	–	**0.83**	–
max.	**1.04**	–	**0.93**	–

Table 2 Main quantities of interest predicted by dynamic and non-dynamic LES and VMS-LES around a circular cylinder at a Reynolds number of 3900. Same symbols as in Table 1.

As previously observed for Re=20000, the Strouhal number is in all cases in good agreement with the reference experimental data and it is not significantly sensitive to grid refinement or SGS modeling. The numerical prediction of the mean drag coefficient is also within the experimental range, except for the no-model simulations giving a small underestimation with respect to the lower bound of the experimental range on both considered grids.

Let us analyze in more details the values obtained for the length of the mean recirculation bubble. As previously mentioned and as also pointed out in the literature (see e.g. [28]), this quantity is difficult to be accurately predicted and it is very sensitive to different simulation parameters. As reference value, we use the one obtained in the experiments in [29], reported in Table 2, which well agrees with the predictions of well resolved LES in the literature (see also the discussion in [28,29]). As can be seen from Table 2, the length of the mean recirculation bubble is noticeably underestimated in all the simulations on the coarser grid GR1. This is in agreement with previous studies [28,3], which indicated that an inadequate grid resolution leads to a too early transition of the shear-layers detaching from the cylinder and, thus, to the formation of the vortices too close to the cylinder; all this results in an underestimation of l_r/D. It was also observed in [3] that the introduction of SGS viscosity in such a situation yields a further reduction of l_r/D and, thus, a further deterioration of the agreement with the experimental reference value. Indeed, paradoxally the *best* prediction on the coarse grid is obtained in the no-model simulation. For both SGS models, the use of the dynamic procedure leads to an increase of l_r/D in LES simulations, although it remains significantly underestimated, while the effects of dynamic SGS modeling on this quantitity are negligible in VMS-LES. On the other hand, for both SGS models, VMS-LES simulations on the finer grid GR2 give values of l_r/D within or very close to the experimental uncertainty range. Once again the impact of dynamic SGS modeling is negligible. Conversely, the no-model simulation on the finer grid gives a noticeable overestimation of l_r/D, confirming once again that in our formulation the numerical viscosity does not mask the effect of SGS models and is not able to replace it. The mean streamwise velocity profile along the wake centerline is reported in Figure 4 for VMS-LES

simulations on the coarse and the fine grids with dynamic and non-dynamic Smagorinsky and WALE models. These profiles confirm the observations previously made for the mean recirculation length.

Analogous considerations can be made by looking at the mean streamwise velocity profiles at different streamwise locations depicted in Figure 5 for the VMS-LES simulations with non-dynamic and dynamic WALE model on the coarse and fine grids. Note, how, on the coarse grid the shape of the profile immediately downstream the cylinder is not correctly reproduced in the simulations (a V shape is obtained instead of the U shape found in the experiments). Also the evolution of the profiles moving downstream is not well predicted. Conversely, the results obtained on the fine grid are in very good qualitative and quantitative agreement with the experimental data. Again, the effect of SGS modeling is very small, as previously in general observed for VMS-LES simulations.

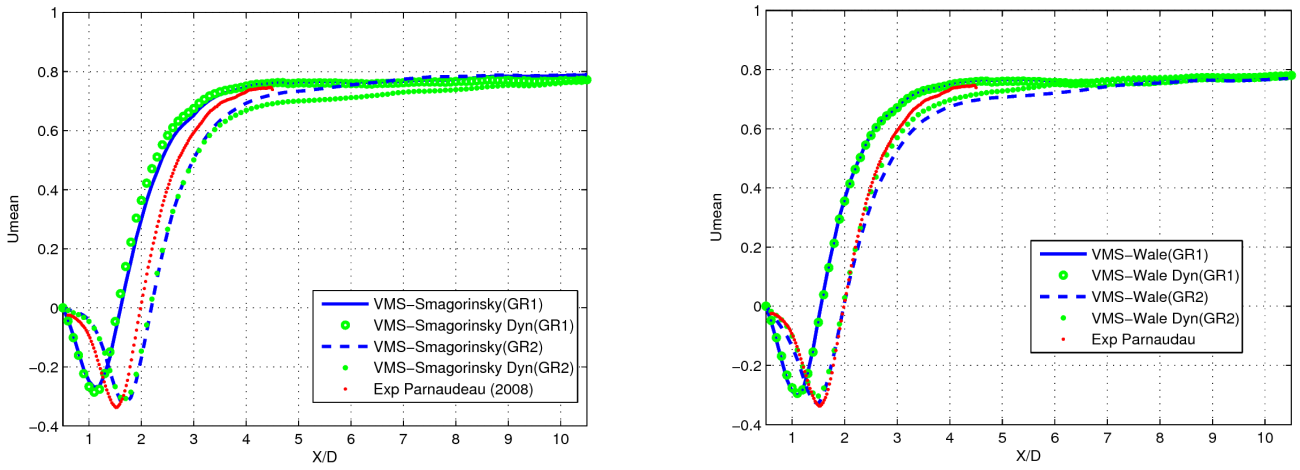

Fig. 4 Flow around a circular cylinder at Reynolds 3900 : mean streamwise velocity profile along the wake centerline for VMS-LES simulations with the Smagorinky model and its dynamic counterpart (a) and with the WALE model and its dynamic counterpart (b) on both grids (GR1 and GR2). The experimental data are taken from [29]. The mean velocity is made nondimensional by means of the freestream velocity.

4.3 Square cylinder flow at Reynolds number 22000

Obstacles with square or rectangular sections are extremely frequent in civil engineering structures, like buildings and bridges. The behavior of a flow past such an obstacle is quite different from the one around a circular cylinder. We restrict here to the case of a zero angle of attack.

Since separation is fixed by geometry, the flow keeps similar properties for a large interval of Reynolds numbers, from 10000 to 200000. This flow configuration is the object of a well-known benchmark [30] at a Reynolds number, based on the cylinder side length, D, and on the freestream velocity, equal to 22000. The overview in [30] points out that, in spite of the fixed separation, this flow is challenging for simulations, the main difficulty being the fact that the boundary layer is laminar when it separates, and transition takes place in the separate free shear layers on the side of the cylinder.

In the present case the computational domain is a cylinder having a circular cross section of radius equal to $R = 15D$ and a spanwise length of $2D$. This length is lower than in DNS in [31] and in [32]; we chose this value after having checked that the results, at least the quantities herein analyzed , do not change significantly compared to those obtained in simulations carried out with a spanwise length of $4D$ as in DNS. The center of the square cylinder cross section coincides with that of the cross section of the computational domain, which is also the origin of the adopted reference frame. The grid is unstructured and has 1.21×10^6 cells; there are 64 nodes on each side of the cylinder and 24 in the spanwise direction uniformly distributed, while the normal distance of the first node layer from the cylinder surface is equal to $2.85 \times 10^{-3}D$. The nondimensional time step is equal to 3.8×10^{-4}, such that there are approximately 500 time steps per shedding cycle. The boundary

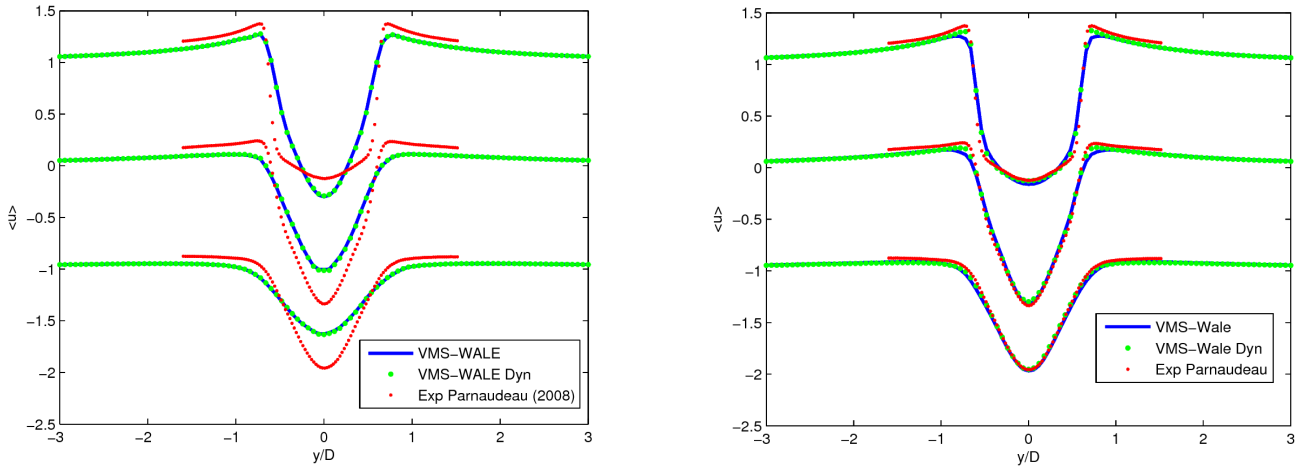

(a) (b)

Fig. 5 Flow around a circular cylinder at Reynolds 3900 : mean streamwise velocity profile at $x/D = 1.06$ (top), $x/D = 1.54$ (center) and $x/D = 2.02$ (bottom), obtained for VMS-LES with dynamic and non-dynamic WALE models on the coarse (a) and fine (b) grids. The experimental data are taken from [29]. The mean velocity is made nondimensional by means of the freestream velocity.

conditions and all the remaining simulation parameters are the same as for the circular cylinder case. For the square cylinder case, we investigate the effects of the dynamic procedure only for the VMS-LES approach with the Smagorinsky model. The results of a simulation with no SGS model are also presented. The time interval used to compute statistics contains 35 vortex-shedding cycles.

	$\overline{C_d}$	l_r/D	St	C'_l	C'_d
VMS Smagorinsky	**2.08**	**0.74**	**0.127**	**1.38**	**0.25**
VMS dyn. Smagorinsky	**2.06**	**0.82**	**0.128**	**1.28**	**0.24**
no model	**1.99**	**0.75**	**0.132**	**1.25**	**0.15**
DNS [31]	**2.09**	–	**0.133**	**1.45**	**0.178**
DNS [32]	**2.1**	–	**0.133**	**1.22**	**0.21**
Exp. [33,34]	**2.1**	**0.88**	**0.132±0.004**	–	–

Table 3 Bulk flow parameters and quantities of interest for the flow around a square cylinder at a Reynolds number of 22000. C'_d is the root mean square of the time fluctuations of the drag coefficient; the other symbols are the same as in previous tables.

In Table 3 we compare a few quantities of interest obtained in our simulations with those of a DNS by Verstappen *et al.*, (from the 1997 paper [31] and from more recent slides [32]) and measurements by Lyn *et al.*, [33,34] and Luo *et al.*, [35].

The DNS simulations in [31,32] and the experiments of [33,34] are characterized by the same blockage factor. Our computational domain has a different shape (circular cross-section instead of rectangular) and its maximum width is significantly larger than that of the DNS. Periodic boundary conditions are used herein as well as in [31,32]; the spanwise length is 4D for the computational domain used in DNS and $9.75D$ in the experiments [33,34]. As for freestream conditions, in our simulations a smooth incoming flow is considered as in [31,32], while the experiments in [33,34] are characterized by a freestream turbulence intensity of 2%. In spite of the previous differences, the DNS results and the experimental data agree very well in the prediction of the Strouhal number and of the mean drag coefficient. Our VMS simulations, both with the non-dynamic and dynamic Smagorinsky models, give predictions of $\overline{C_d}$ in good agreement with the literature data, while the no-model simulation slightly underestimates it. As for the Strouhal number, all the values are within or very close to the experimental range and this quantity is only slightly sensitive to SGS modeling, as expected in this case since the boundary-layer separation is fixed by the geometry. Conversely, the r.m.s. of the time fluctuations of lift and drag coefficient vary more significantly with SGS modeling; however, it is

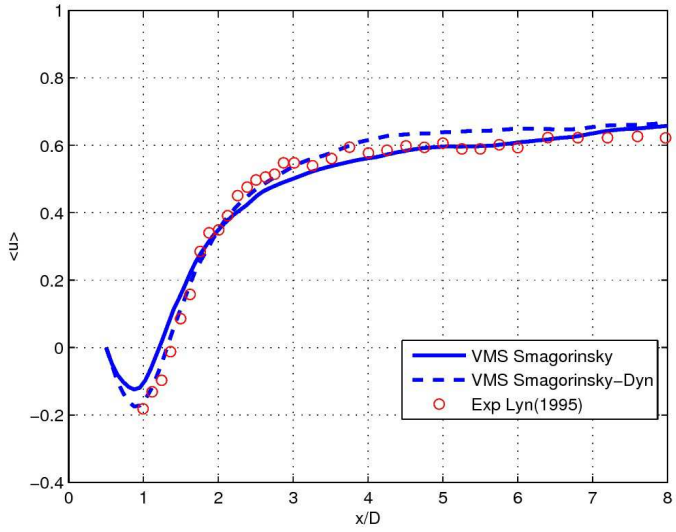

Fig. 6 Flow around a square cylinder at Reynolds 22000 : mean streamwise velocity on the centerline of the wake. Experimental data are taken from[34]. The mean velocity is made nondimensional by using the freestream velocity.

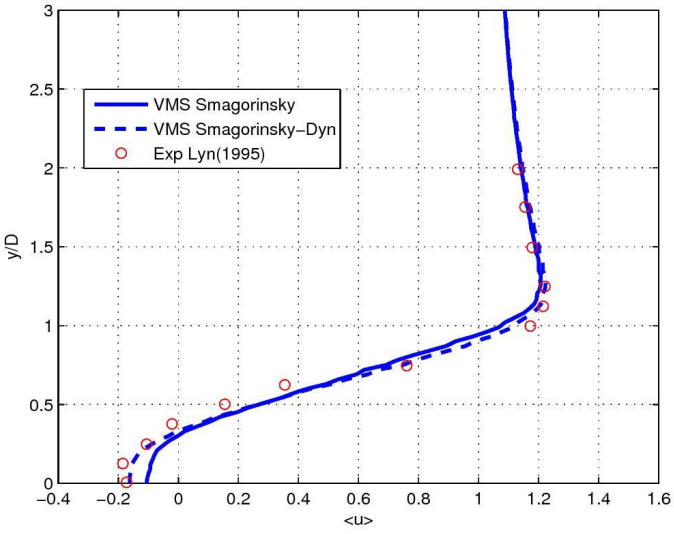

Fig. 7 Flow around a square cylinder at Reynolds 22000 : mean streamwise velocity at x/D=1. Experimental data are taken from[34]. The mean velocity is made nondimensional by using the freestream velocity.

hard to draw some conclusions on these quantities since also in DNS in [31] and [32]significantly different values are obtained. Finally, as previously observed for the circular cylinder case, another quantity which is significantly sensitive to SGS modeling is the length of the mean recirculation bubble. The best agreement with the experimental value is obtained in the VMS-LES simulation with the dynamic Smagorinsky model. This can be seen also in Fig. 6, which shows the mean streamwise velocity along the wake centerline. The mean velocity field in the near-wake obtained with the dynamic Smagorinsky model is in general in better agreement with the experimental one than that given by the non-dynamic one; this can be seen again in Fig. 6, by looking for instance at the prediction of the mean velocity in the recirculation zone, or in Fig. 7, showing the mean streamwise velocity profile immediately downstream the cylinder ($x/D = 1$). Conversely, the use of dynamic SGS modeling does not affect the main velocity filed on the lateral sides of the cylinder, as shown for instance by the mean streamwise velocity profile at $x/D = 0$ reported in Fig. 8. Note also how there is

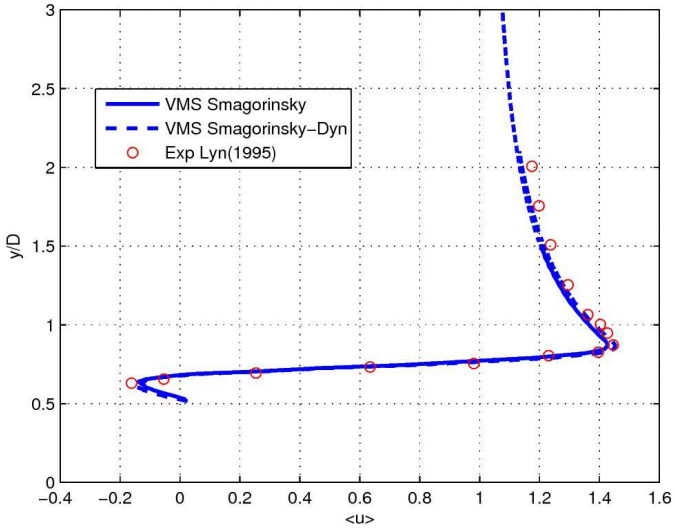

Fig. 8 Flow around a square cylinder at Reynolds 22000: mean streamwise velocity at x/D=0. Experimental data are taken from [34]. The mean velocity is made nondimensional by using the freestream streamwise velocity.

good agreement between the numerical and experimental values of the mean streamwise velocity also quite far from the cylinder surface; therefore, it can be inferred that the different blockage does not seem to significantly affect the mean velocity field around the cylinder.

4.4 Square cylinder flow at Reynolds number 175000

Let us briefly analyze, finally, the flow around the square cylinder at Re=175000. We use the same computational domain, the same grid and the same simulation set up, except for the Reynolds number value, as in Sec.4.3. Table 4 shows some quantities of interest obtained for this flow with our simulations, and the data from the experiments in [36] and [37]. These experiments are characterized by a blockage factor of 3.6% and of 7% and by an aspect ratio of $9.2D$ and $14D$ respectively. In both cases, the results for smooth incoming flow are considered. The mean drag coefficient is not very different from the one at Re=22000 reported in Table 3, as it was expected for this kind of flow. A good agreement with the experimental value is obtained in the VMS-LES simulations, both with dynamic and non-dynamic SGS Smagorinsky models, while in the no-model simulation it is noticeably underestimated. Similar considerations can be made for the base pressure, and for the r.m.s. of the time fluctuations of the drag and lift coefficient. The Strouhal number is overestimated in all the simulations; the best agreement is obtained with the dynamic Smagorinsky model, with a difference of 4%. Finally, as for l_r/D, the values obtained in the VMS-LES simulations are similar, while the no-model one gives a larger prediction. We could not find an experimental value for this quantity at this Reynolds number, but its value is expected to decrease compared with the previous Reynolds number. Consistently, the VMS-LES with the Smagorinsy model and, more significantly, the one with the dynamic version give a lower value than at Re=22000 (compare Tables 4 and 3), while the no-model simulations show the opposite trend.

5 Conclusions

A variational multiscale LES approach combined with dynamic SGS models has been presented. The VMS approach and the dynamic procedure may a-priori be considered complementary, since the first selects which scales are damped by the SGS viscosity and the latter the regions in which damping is applied at different time instants. In this paper we propose a dynamic procedure which implies very low additional costs also for unstructured grids and we appraise the impact of dynamic SGS modeling in classical LES and VMS-LES of bluff-body flows in subcritical regime. More specifically, the flow around a circular cylinder at Reynolds

	$\overline{C_d}$	l_r/D	St	C'_l	C'_d	$-\overline{C}_{pb}$
VMS Smagorinsky	**2.03**	**0.73**	**0.129**	**1.29**	**0.26**	**1.30**
VMS dyn. Smagorinsky	**2.03**	**0.75**	**0.127**	**1.26**	**0.23**	**1.30**
no model	**1.86**	**0.81**	**0.132**	**1.09**	**0.11**	**1.38**
Exp. [36]	**2.06**	–	**0.122**	**1.21**	**0.23**	**1.30**
Exp. [37]	–	–	**0.12**	**1.32**	–	–

Table 4 Bulk flow parameters predicted by dynamic and non-dynamic VMS-LES around a square cylinder at a Reynolds number of 175000. Same symbols as in previous tables.

numbers 3900 and 20000 and the flow around a square cylinder at Reynolds 22000 and 175000 have been considered as benchmark tests.

The key ingredients of the numerics and modeling used in this work are the following: unstructured grids, a second-order accurate numerical scheme stabilized by a tunable numerical diffusion proportional to sixth-order space derivatives, and the VMS formulation combined with the dynamic and non-dynamic Smagorinsky and WALE SGS models. A set of rather coarse unstructured grids, as those often used in industrial applications, have been used, in order to have a significant impact of SGS terms of the flow dynamics. This has been confirmed by simulations carried out without any SGS model, which showed, in agreement with what observed in our previous studies, that the numerical viscosity used in our formulation does not mask the effects of SGS models.

As a first remark, we observed that the dynamic procedure significantly reduces the amount of introduced SGS viscosity with respect to that given by non-dynamic SGS models, both in classical and VMS LES simulations. However, it has been found that, when combined with the VMS-LES approach, the dynamic procedure has a smaller impact on bulk coefficients and main flow features than when used with a classical LES, which partly confirms the conclusions of previous works. This may be explained by the fact that the SGS viscosity only acts on the smallest resolved scales in the VMS-LES approach, while this viscosity applies to all the resolved scales in classical LES models. For classical LES, the dynamic procedure generally leads, as expected, to a better agreement with literature reference data. In VMS-LES, as previously said, the impact of dynamic SGS modeling is in most cases and for most quantities very small, but almost never leads to a deterioration of the agreement with reference data. Conversely, in some cases and for the Smagorinsky model, it leads to a significant improvement of this agreement; this happens, for instance, for the prediction of the turbulence intensity along the wake axis in the flow around the circular cylinder at $Re = 20000$ or of the mean velocity field in the near wake of the square-cylinder flow at $Re = 22000$.

Therefore, with a careful implementation leading to negligible additional costs of the dynamic procedure, as the one used in the present work, dynamic models may be considered an interesting option also within the VMS-LES approach.

Acknowledgements This work has been supported by French National Research Agency (ANR) through COSINUS program (project ECINADS n^o ANR-09-COSI-003). HPC resources from GENCI-[CINES] (Grant 2010-x2010026386 and 2010-c2009025067) are also gratefully acknowledged.

References

1. P. Sagaut, *Large eddy simulation for incompressible flows*. Third Edition, Springer-Verlag, Berlin-Heidelberg, 2006.
2. S. Camarri, M.V. Salvetti, B. Koobus, and A. Dervieux. A low diffusion MUSCL scheme for LES on unstructured grids. *Comp. Fluids*, 33:1101-1129, 2004.
3. H. Ouvrard, B. Koobus, A. Dervieux, and M.V. Salvetti. Classical and variational multiscale LES of the flow around a circular cylinder on unstructured grids. *Computer and Fluids*, 39(7):1083-1094, 2010.
4. S. Wornom, H. Ouvrard, M.-V. Salvetti, B. Koobus, A. Dervieux. Variational multiscale large-eddy simulations of the flow past a circular cylinder : Reynolds number effects. *Computer and Fluids*, 47(1):44-50, 2011.
5. T.J.R. Hughes, L.Mazzei, and K.E. Jansen. Large-eddy simulation and the variational multiscale method. *Comput. Vis. Sci.*, 3:47-59, 2000.
6. J. Smagorinsky, General circulation experiments with the primitive equations. *Month. Weath. Rev.*, 91(3) :99-164, 1963.
7. F. Nicoud and F. Ducros. Subgrid-scale stress modelling based on the square of the velocity gradient tensor. *Flow Turb. Comb.*, 62(3):183-200, 1999.
8. B. Koobus and C. Farhat. A variational multiscale method for the large eddy simulation of compressible turbulent flows on unstructured meshes-application to vortex shedding. *Comput. Methods Appl. Mech. Eng.*, 193:1367-1383, 2004.
9. M. Germano, U. Piomelli, P. Moin, W.H. Cabot. A Dynamic Subgrid-Scale Eddy Viscosity Model. *Physics of Fluids*, A 3, 1760-1765, 1991.

10. C. Farhat, A. Rajasekharan, B. Koobus. A dynamic variational multiscale method for large eddy simulations on unstructured meshes. *Comput. Methods Appl. Mech. Engrg.*, 195 (2006) 1667-1691.
11. J. Holmen, T.J.R. Hughes, A.A. Oberai, GG.N. Wells. Sensitivity of the scale partition for variational multiscale LES of channel flow. *Phys. Fluids*, 16(3) (2004) 824-b27.
12. V. Gravemeier. Variational Multiscale Large Eddy Simulation of turbulent Flow in a Diffuser. *Computational Mechanics*, 39(4):477:495, 2012.
13. M.H. Lallemand, H. Steve, and A. Dervieux. Unstructured multigridding by volume agglomeration : current status. *Comput. Fluids*, 21:397-433, 1992.
14. D. K. Lilly. A proposed modification of the Germano subgrid scale closure model. *Physics of Fluids A*, 4:633-635, 1992.
15. H. Baya Toda, K. Truffin and F. Nicoud. Is the dynamic procedure appropriate for all SGS model. *V European Conference on Computational Fluid Dynamics*, ECCOMAS CFD, J.C.F. Pereira and A. Sequeira (Eds), Lisbon, Portugal, 14-17 June 2010.
16. C. Farhat, B. Koobus and H. Tran. Simulation of vortex shedding dominated flows past rigid and flexible structures.*Computational Methods for Fluid-Structure Interaction*, 1-30, 1999.
17. P. L. Roe. Approximate Riemann solvers, parameters, vectors and difference schemes. *J. Comp. Phys*, 43:357-371, 1981.
18. B. Van. Leer. Towards the ultimate conservative scheme. IV :A new approach to numerical convection. *J. Comp. Phys.*, 23:276-299, 1977.
19. R. Martin and H. Guillard. A second-order defect correction scheme for unsteady problems. *Comput. and Fluids*, 25(1):9-27, 1996.
20. J.L. Steger, R.F. Warming. Flux vector splitting for the inviscid gas dynamic equations with applications to the finite difference methods. *J. Comp. Phys.*, 40(2):263-293, 1981.
21. E. Salvatici and M.V. Salvetti, Large-eddy simulations of the flow around a circular cylinder: effects of grid resolution and subgrid scale modeling, *Wind & Structures*, 6(6):419-436, 2003.
22. S. Aradag. Unsteady turbulent vortex structure downstream of a three dimensional cylinder, *J. of Thermal Science and Technology*, 29(1):91-98, 2009.
23. H. Lim and S. Lee. Flow Control of Circular Cylinders with Longitudinal Grooved Surfaces, *AIAA Journal*, 40(10):2027-2035, 2002.
24. J.D. Anderson. *Fundamentals of Aerodynamics*, Second Edition, McGraw-Hill, New York, 1991.
25. C. Norberg. Fluctuating lift on a circular cylinder: review and new measurements. *J. Fluids Struct.*, 17:57-96, 2003.
26. C. Norberg. Pressure distribution around a circular cylinder in corss-flow. *Proceedings of the Symposium on bluff body wakes and vortex-induce vibrations (BBVIV3)*, K. Hourigan, Leweke T., Thompson M.C. and Williamson C.H.K. Eds., Port Arthur, Quuensland (Australia), 2002.
27. L. Ong and J. Wallace. The velocity field of the turbulent very near wake of a circular cylinder. *Exp. Fluids*, 20: 441-453, 1996.
28. A.G. Kravchenko and P. Moin. Numerical studies of flow over a circular cylinder at re=3900. *Phys. Fluids*, 12(2):403-417, 1999.
29. P. Parnaudeau, J. Carlier, D.Heitz and E. Lamballais. Experimental and numerical studies of the flow over a circular cylinder at Reynolds number 3900. *Phys. Fluids*, 20(085101), 2008.
30. W. Rodi, J.H. Ferziger, M. Breuer and M. Pourqui "Status of Large Eddy Simulation: Results of a Workshop" *J. Fluids Engineering*, Transactions of the ASME, 119, 248-262, (1997).
31. R.W.C.P. Verstappen and A.E.P. Veldman, Direct numerical simulation of turbulence at lower costs. *Journal of Engineering Mathematics*, 32:143-159, 1997.
32. R. Verstappen. Regularizing turbulent flow, 2010. *http://www.prace-ri.eu/IMG/pdf/16-verstappen.pdf*
33. D. A. Lyn and W. Rodi The flapping shear layer formed by flow separation from the forward corner of a square cylinder *J. Fluid Mech.* 261:353-316, 1994.
34. D. A. Lyn, S. Einav, W. Rodi and J-H. Park, A laser-Doppler velocimetry study of ensemble-averaged characteristics of the turbulent near wake of a square cylinder. *J . Fluid Mech.* 304:285-319, 1995.
35. S. C. Luo and MdG. Yazdani and Y. T. Chew and T. S. Lee, Effects of incidence and afterbody shape on flow past bluff cylinders, *J. Ind. Aerodyn.*, 53:375-399, 1994.
36. B.E. Lee, The effect of turbulence on the surface pressure field of a square prism. *J. Fluid Mech.*, 69:263-282, 1975.
37. B.J. Vickery. Fluctuating lift and drag on a long cylinder of square cross-section in a smooth and in a turbulent stream. *Fluid Mech*, 25:481-494, 1966.